Experimental characterization and thermoviscoelastic modeling of strain and stress recoveries of an amorphous polymer network

J. Sebastián Arrieta[1,*], Julie Diani, Pierre Gilormini

Laboratoire PIMM, CNRS, Arts et Métiers ParisTech, 151 bd de l'Hôpital, 75013 Paris, France

Abstract

An acrylate polymer network was submitted to thermomechanical shape memory cycles. The set of experiments characterized the material stress-free strain recovery and the strain-constrained stress recovery in uniaxial tension. Experimental parameters like temperature of strain fixation, amount of strain and heating rate, were varied in order to provide a relatively complete set of experimental data. A model combining the amorphous polymer viscoelasticity and its time-temperature superposition property was used to predict the shape memory behavior of the acrylate polymer network. All the model parameters were characterized using classical tests for mechanical characterization of polymers, which do not include shape memory tests. Model predictions obtained by finite element simulations compared very well to the experimental data and therefore the model relevance for computer assisted application design was assessed.

Keywords: Shape memory, B: finite strain, B: viscoelastic material, B: polymeric material, C: mechanical testing

1. Introduction

Shape memory polymers find applications in space systems, solar panels, textiles, and largely in medical devices. For computer assisted application design, it is critical for the engineer to have constitutive equations that represent

*Corresponding author. Tel. : + 33 1 44 24 61 92; fax: + 33 1 44 24 62 90.
Email address: juan-sebastian.arrieta-escobar@ensam.eu (Sebastián Arrieta)

well the material behavior with respect to time and temperature. Despite that fact, the number of papers dedicated to modeling shape memory polymers remains limited. We may divide the existing models into two categories: the models based on a bi-phasic representation of the material grounded on the rubbery/glassy state transition, first proposed by Liu et al. (2006) and adopted by Chen and Lagoudas (2008), Qi et al. (2008), Volk et al. (2010), Gilormini and Diani (2012), and the thermoviscoelastic approach early introduced by Tobushi et al. (1997) and improved by Diani et al. (2006), Nguyen et al. (2008), Castro et al. (2010), Srivastava et al. (2010), Diani et al. (2012) and Yu et al. (2012).

Recently, Diani et al. (2012) showed that an epoxy network submitted to torsion shape recovery tests in large-deformation small-strain conditions, could be well predicted by simply introducing the material linear viscoelastic parameters into the large-deformation viscoelastic framework of Simo (1987) coupled with the material time-temperature superposition property. The model attributes the shape memory property of amorphous polymer networks to their viscoelasticity combined with time-temperature superposition. The model showed very good predictions of the kinetics of the shape recovery and presents the great interest to depend on parameters that can be determined by standard polymer characterization tests only. Nonetheless, the model had been only applied to small-strain shape recovery (strain $<10\%$) and its ability to predict the stress history vs. time and temperature had not been tested yet. In this contribution, a complete set of strain and stress recoveries obtained during classical shape memory thermocycles is presented. For this purpose, an acrylate polymer network was synthesized and submitted to thermomechanical cycles consisting in applying a uniaxial strain at high temperature, cooling down the material while maintaining the strain, releasing the stress and finally heating the sample stress-free or strain-constrained. Several experimental parameters were varied like the heating rate, the temperature of temporary strain fixation, and the amount of applied stain. The comparison between the model prediction and the experimental data assesses the model relevance for amorphous polymer networks shape memory application design.

2. Mechanics of the material

2.1. Material

The acrylate network composition was found in Safransky and Gall (2008). It was prepared by the copolymerization of benzyl methacrylate (BMA) with poly(ethylene glycol) dimethacrylate (PEGDMA) of molar weight 550 g/mol, which is used as crosslinking agent. 2,2-dimethoxy-2-phenylacetophenone (DMPA) was added as photoinitiator. Products were used as received from Sigma Aldrich. 90% molar mass of BMA was mixed at room temperature with 10% molar mass of PEGDMA and 0.5% of DMPA. The mix was cured in a UVP® ultraviolet chamber CL-1000 for 50 minutes. Final products are plates of 1.3 mm thickness from which dumbbell and rectangular samples are cut for thermomechanical tests and analysis.

2.2. Mechanical behavior characterization

The material viscoelasticity was characterized by tensile dynamic mechanical analysis (DMA) performed on a DMA Q800 from TA instruments. The material was submitted to isothermal frequency sweeps at 0.1% strain from 0.01 to 10 Hz, from 0°C to 65°C with 5°C increments. The material viscoelasticity master curves shown in Figure 1 were obtained from the DMA tests by applying the time-temperature superposition principle at the reference temperature of 80 °C. The horizontal shift factor a_T values used to build the master curves in Figure 1 were found to satisfy the WLF equation of Williams et al. (1955):

$$\frac{1}{log_{10}(a_T)} = \frac{-1}{C_1} - \frac{C_2}{C_1}\frac{1}{T - T_{ref}} \tag{1}$$

with $C_1 = 6.9$ and $C_2 = 87.9$°C for $T_{ref} = 80$°C.

The material was also submitted to conventional uniaxial tension tests at various temperatures, using an Instron® 5881 testing machine equipped with a thermal chamber. Local strain measures were recorded by video extensometry. Tests were run at a constant crosshead speed of 10 mm/min. Figure 2(a) presents the material stress-strain responses to monotonic loadings until break at a low temperature (25°C) corresponding to the glassy state, at a high temperature (65°C) corresponding to the rubbery state, and at an intermediate temperature (45°C) at which the material is strongly viscoelastic. In the glassy state, the material presents a classic elasto-plastic behavior. In the rubbery state, it undergoes large strains and exhibits a hysteretic loop

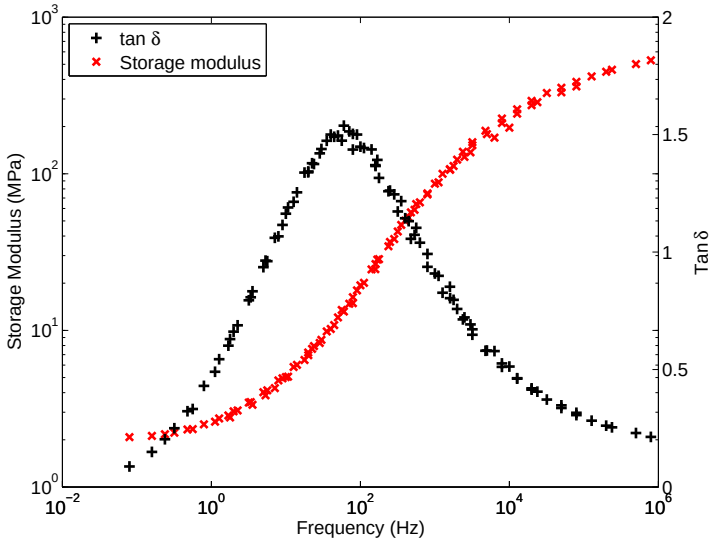

Figure 1: Storage Young modulus and loss tangent angle master curves of the acrylate at the reference temperature $T_{ref} = 80°C$, obtained from the time-temperature superposition principle applied to the DMA tensile tests.

when submitted to a cyclic test (Figure 2(b)). This phenomenon is enhanced in the viscoelastic transition (45°C). At this temperature, the residual strain is completely recovered at zero stress within two hours but the material response at the second load is different from the first load. This material feature was obtained consistently. Moreover, this behavior at second load is also obtained when relaxing the residual strain at 65°C rather than 45°C. Such a hysteresis disappears when tests (not shown) are run at the slower crosshead speed of 1 mm/min. At the intermediate temperature of 45°C, the material presents also enhanced strain to failure (Figure 2(a)), which may be interesting for large deformation storage during shape memory thermocycles. The strain to failure enhancement, when temperature varies within the glass transition, had been reported in the works of Smith (1963) in a elastomer and in the works of Yackaki et al. (2008) and of Safransky and Gall (2008) in a shape memory polymer acrylate network. Actually, Rousseau and Xie (2010), Feldkamp and Rousseau (2011) and Leonardi et al. (2011) have shown that it is possible to store and recover a deformation applied at temperatures well below the rubbery state.

The acrylate thermal expansion coefficient $\alpha(T)$ was measured by dilatometry with a Netzsch® TMA 402 F3 Hyperion device. The material linear

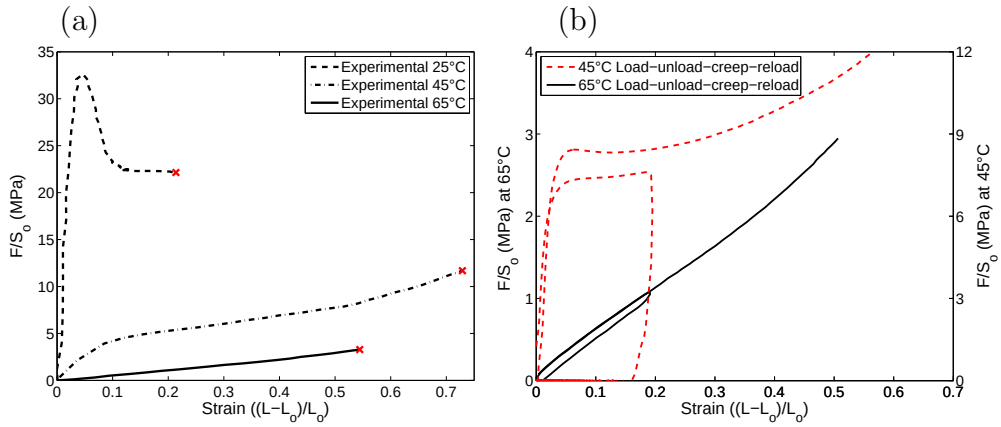

Figure 2: Material uniaxial stress-strain responses for various temperatures during (a) monotonic tests and (b) cyclic tests defined by load, unload, residual strain recovery at zero stress and reload. Crosshead speed: 10 mm/min.

expansion was measured as a function of temperature for two different heating ramps (1°C/min and 5°C/min). The thermal procedure was to heat the sample up to 80°C, then to cool it down to 0° and to heat the sample again. Figure 3 shows the evolution of the dilation and the expansion coefficient measured as the samples were heated from 0 to 80°C. From figure 3, the material shows a thermal expansion glass transition temperature of 39°C at 1°C/min and of 37°C at 5°C. One may notice the impact of the heating rate on the expansion coefficient.

3. Thermomechanical cycle tests

3.1. Test presentation

The material behavior during thermomechanical shape memory cycles is studied in uniaxial tension. The experimental set up is the same as used for the mechanical tests. The temperature history is recorded with three thermocouples connected to a computer through the myPCLab data acquisition tool from NOVUS. The shape memory tests consist of the deformation and fixation of a temporary shape in uniaxial tension, and the subsequent free length or constrained length recovery when samples are subjected to a constant heating ramp. Therefore, we will differentiate two kinds of recoveries, the free length recovery for which the uniaxial strain is recorded as the sample is stress-free, and the constrained length recovery for which the

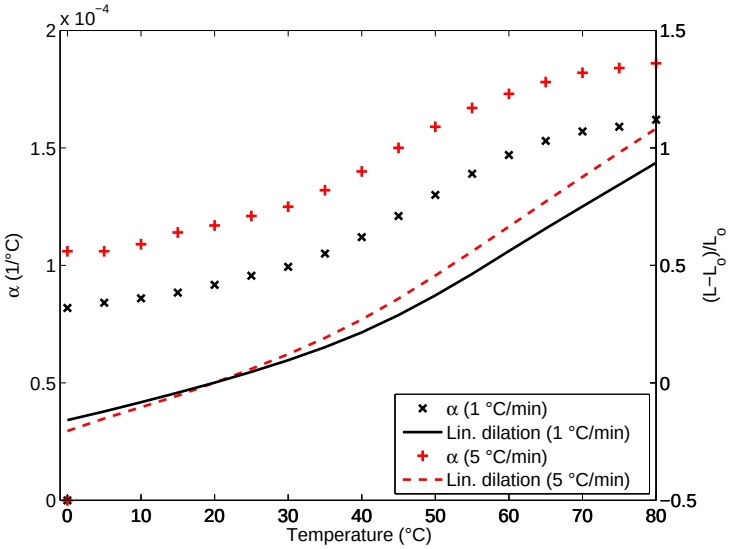

Figure 3: Thermal expansion measured during sample heating at 1°C/min and 5°C/min.

uniaxial stress is recorded as the sample length is maintained constant. Test procedures are represented in the space of strain, stress and temperature in Figure 4. The corresponding procedure steps are enumerated below:

1. Temporary shape application step: a uniaxial tensile deformation is applied at a high temperature.
2. Temporary shape fixation step: the deformed sample is cooled down to room temperature while uniaxial strain is maintained constant.
3. Stress release step: the uniaxial stress is set to zero at room temperature.
4. Recovery step: the sample is submitted to a constant heating rate, being either (a) free of stress and the strain recovery is measured, or (b) constrained in length and the stress recovery is recorded (Figure 4).

In order to propose a relatively complete study of the material behavior during the thermomechanical recovery tests, we varied some of the test parameters. During step 1, the temporary uniaxial strain was applied at 45°C or 65°C and reached 20% or 50%. During step 4, the heating rate was set to 1°C/min or 5°C/min. Each sample is submitted to the complete thermomechanical cycle but the next two sections present the experimental data recorded during step 4 only.

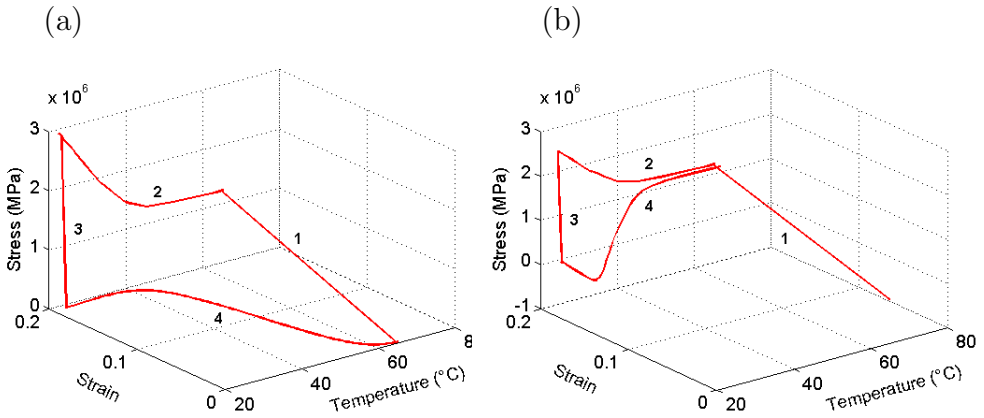

Figure 4: Thermomechanical recovery test representation: (1) uniaxial tension at high temperature, (2) cooling down to room temperature at constant strain, (3) uniaxial stress release, and (4) sample heating at constant heating rate, with either (a) stress-free length recovery or (b) constrained length stress recovery.

3.2. Free length recovery

This section is dedicated to the uniaxial strain recovery measures obtained during stress-free sample heating. The effects of three loading conditions on the strain recovery are studied: the heating rate, the deformation temperature, and the deformation magnitude.

First, the material is submitted to a 20% strain at 65°C, a temperature at which the material is in its rubbery state. Figure 5 shows the material strain recoveries for temperature ramps of 1°C/min and 5°C/min. As expected for a thermoset deformed in its rubbery state, a complete strain recovery is observed. Moreover, the strain recovery shifts toward higher temperatures when increasing the heating ramp. This effect has already been reported on epoxy networks by Rousseau and Xie (2010) in uniaxial tension and by Diani et al. (2012) in torsion.

Second, the effect of the temperature of temporary shape fixation on the strain recovery kinetics is presented in Figure 6. Samples were submitted to a 20% pre-strain at 45°C or 65°C. At 45°C, the material is not in the rubbery state, and Figure 2 already showed that the material behavior differs significantly at such a temperature from its behavior at 65°C. Nonetheless, Figure 6 shows similar strain recoveries for samples pre-strained at 45°C or 65°C.

Finally, since larger strain can be achieved at 45°C, some samples were

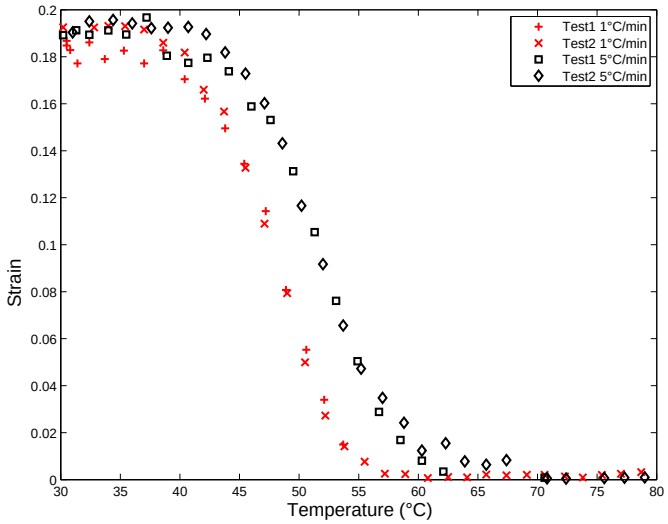

Figure 5: Free length recovery with respect to temperature for 20% pre-deformed samples at 65 °C and heated at 1 or 5 °C/min.

submitted to 50% strain fixation and their strain recoveries were compared to the recoveries of samples submitted to 20% strain at the same temperature. The strain recovery appears as complete for 50% strain as for 20% strain (Figure 7), with very similar evolutions when the strain is normalized by the pre-strain value.

3.3. Constrained length recovery

Constrained length recovery tests are dual to strain recovery tests. During the former, the specimen length is maintained constant while heating the sample and recording the stress vs. temperature. First, stress recoveries were recorded for samples submitted to a pre-strain of 20% at 65°C and heated at 1°C/min and 5°C/min. Figure 8 presents the evolution of the engineering uniaxial stress (F/S_o) with respect to temperatures. At low temperatures, the compressive stress results from the restrained thermal expansion. At higher temperatures, the material undergoes a state transition from the glassy state to the rubbery state, which causes a change into the stress evolution toward positive values. In the rubbery state, the stress converges toward the value corresponding to the material mechanical strain-stress response, i.e. ≈1MPa for 20% strain (Figure 2). The observed dependence of the stress response on the heating rate is in accordance with the previous works of

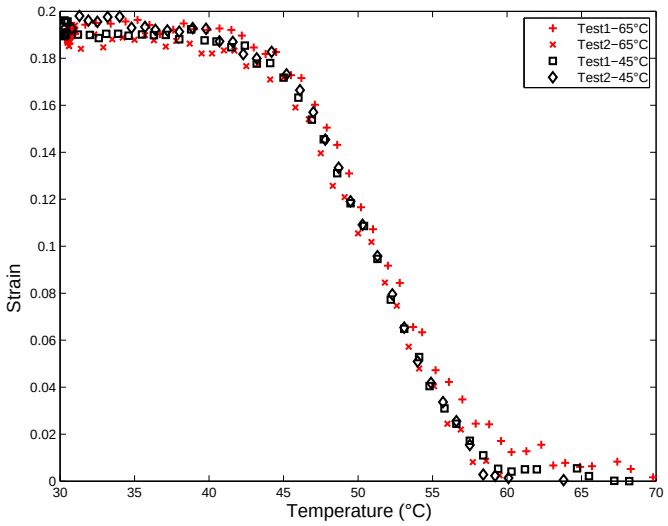

Figure 6: Free length recovery vs. temperature of samples 20% pre-strained at 45 or 65°C and heated at 5 °C/min.

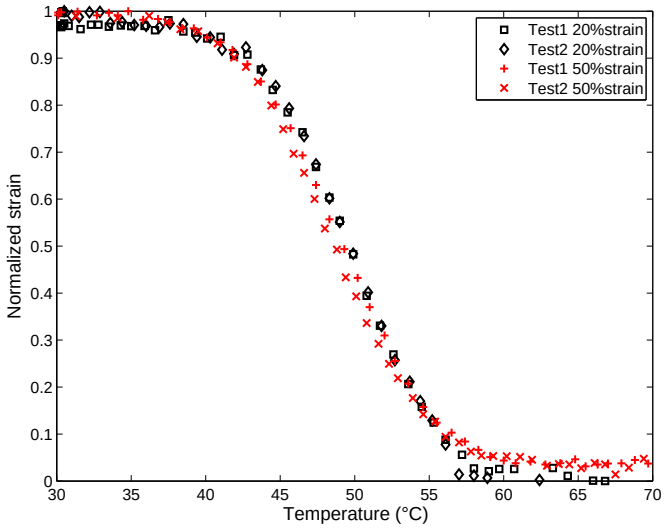

Figure 7: Normalized free length recovery vs. temperature of samples 20% or 50% pre-strained at 45 °C and heated at 5 °C/min.

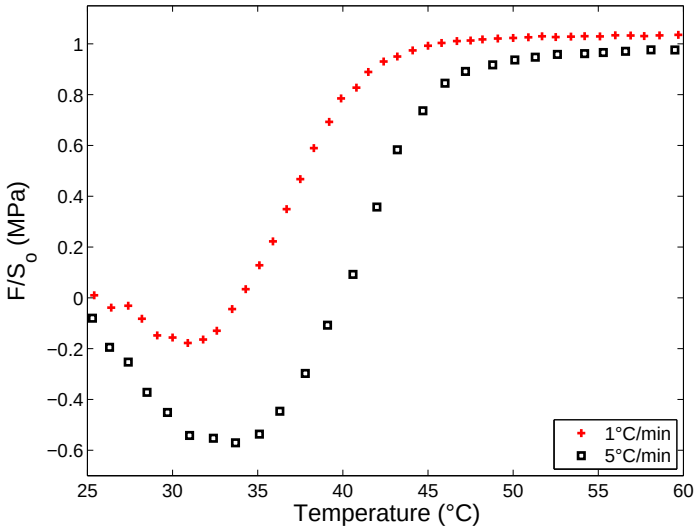

Figure 8: Influence of the heating rate on constrained length recovery for samples 20% pre-deformed at 65 °C and heated at 1 °C/min or 5 °C/min

Nguyen et al. (2008) and Castro et al. (2010). The larger compression stress recorded during the test run at 5°C/min is consistent with the dependence of the material thermal expansion coefficient on the heating rate displayed in Figure 3.

Second, stress recoveries were recorded for samples uniaxially strained at 45°C to 20% and 50%. Figure 9 presents the stress evolutions with respect to temperature. When comparing Figures 8 and 9, the strong impact of the temperature of strain fixation on the constrained length stress recovery can be noted. When the material is pre-strained while not in the rubbery state, the stress recoveries present a small compressive state at low temperatures, which fades away if the material had been substantially deformed. At higher temperatures, the uniaxial stress becomes positive, as expected from the material change of state. More interestingly, the stress presents an overshoot before tending toward the rubbery state response at high temperatures. Such a stress overshoot was reported by Gall et al. (2005) and Azra et al. (2011) for similar test conditions. Note that like for samples pre-strained at 65°C, the stress reaches the value corresponding to the stress-strain response in the rubbery state (Figure 2b). This feature was also reported by Gall et al. (2005) and Azra et al. (2011).

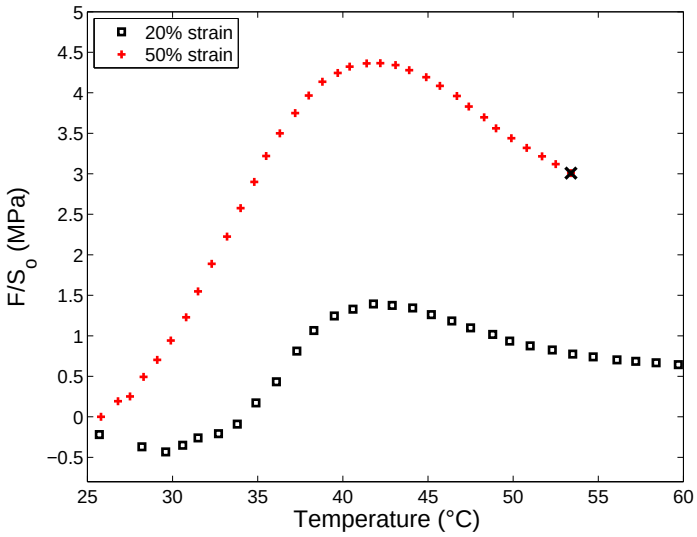

Figure 9: Constrained length recovery for samples pre-deformed at 20% and 50% strain at 45 °C and heated at 1 °C/min

4. Modeling

4.1. Model

Recently, Diani et al. (2012) proposed to apply the generalized finite deformation viscoelasticity theory of Simo (1987) coupled to the general time-temperature superposition property of amorphous networks to model the shape recovery of an epoxy network. The mechanical behavior parameters are defined by the material linear viscoelasticity characterized by dynamic mechanical analysis at infinitesimal strain, and by the material hyperelasticity measured by a standard uniaxial tension test at high temperature. The model showed excellent predictions of deformation recoveries with respect to temperature for relatively small-strain large-deformation torsion tests. It is now applied to large uniaxial strain and confronted to not only strain recovery but also stress recovery.

The material time-temperature superposition property is well approached by the WLF relation (Eq. (1)). The material linear viscoelasticity presented in Figure 1 is well reproduced by a generalized Maxwell model (Figure 10), which 20 relaxation times and Young moduli are calculated with the procedure of Weese (1993). Assuming quasi-incompressibility, the material hyperelastic response, as characterized with slow strain rate uniaxial tests run at

65°C, is well modeled by a simple neo-Hookean behavior $\sigma = 2C_{10}(\lambda^2 - \lambda^{-1})$ with σ the Cauchy stress and λ the uniaxial stretch, with $C_{10} = 1.1$ MPa.

Despite the fact that only uniaxial state of strain are considered in this study, the model was implemented in Abaqus (Abaqus/Standard (2010)) for two reasons: (i) the constitutive equations are already programmed in the finite element software and therefore require an easy and standard use of the code, and (ii) the large number of relaxation times (20) required to provide a precise material thermoviscoelastic response renders the model programming tedious. The model parameters are given in the Appendix as written in the Abaqus input file. Note that in Abaqus the `*VISCOELASTIC` option requires the shear relaxation moduli G_i instead of the Young modulus relaxation moduli E_i provided by the generalized Maxwell model fit shown in Figure 10. Therefore, G_i values were calculated from the E_i values assuming the bulk modulus is independent of temperature and equal to $B = 1130$ MPa. The latter value corresponds to a Poisson's ratio of $\nu = 0.41$ in the glassy state and $\nu \simeq 0.5$ in the rubbery state. Albeit B is known to vary with temperature (but much less than the Young modulus), it seems fair to assume that the impact of this variation on the material uniaxial thermoviscoelastic response is limited. The good accordance between the model and the experiments will validate this assumption in the following. In order to account for the variations of the material thermal expansion coefficient with heating rate and temperature, the measured values (Figure 3) of this parameter every 5°C were used in the simulations. It should be noted that the model has no adjustable parameter and that its parameters are not fitted on shape memory thermomechanical cycle tests but on tests routinely run for polymer characterization. For each experimental recovery test, the whole thermomechanical cycle (detailed in section 3.1) is simulated with the measured temperature history given as an input in the calculations. The resulting strain or stress recovery obtained during the fourth step of the thermomechanical cycle is then compared to the experimental measures.

4.2. Results

Figure 11 compares the model predictions and the material strain recoveries with respect to temperature for two heating rates, for samples pre-strained at 65°C. An excellent agreement between the model and the experiments can be noted, which extends the model applicability to large-strain. Figure 12 presents the model predictions of the stress recoveries of samples pre-strained at 65°C at two different heating rates. From Figures 11 and 12, the model

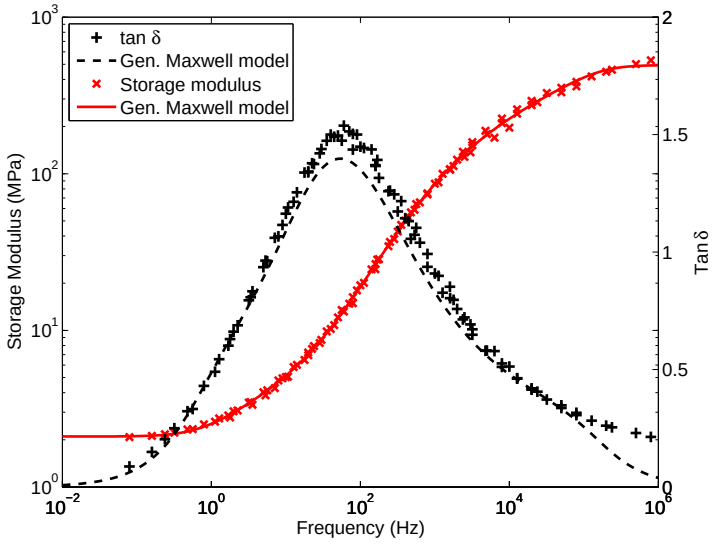

Figure 10: Approximation of the material linear viscoelasticity by a generalized Maxwell model

is shown to predict the material trend to shift the strain free and stress free recovery curves when the heating rate is increased. Note that for these test simulations, it is important to account for the thermal expansion coefficient dependences on temperature and heating rate in order to reproduce the compressive part of the stress measurements satisfactorily.

In Figure 13, the model demonstrates a good ability to predict the material strain recovery with respect to temperature for samples submitted to strain fixation at 45°C. Nonetheless, the model predictions are less accurate than those obtained for samples pre-strained at 65°C (Figure 11). Remind that model parameters at low temperatures come from linear viscoelasticity only, and therefore all the relevant behavior parameters for large strain at low temperatures may not be included.

Figure 14 presents the model predictions of the stress recoveries obtained for samples pre-strained at 45°C at 20% and 50%. The model shows very satisfactory predictions of the material response for a 20% pre-strain. The model prediction of stress recovery after 50% pre-strain shows some discrepancy with the actual response, but the overall shape of the stress-temperature curve is reproduced quite well and the stress peak value is correct. This peak value is very sensitive to the duration of the stress relaxation applied at 45°C after stretching and before cooling. Therefore, the duration of every step of

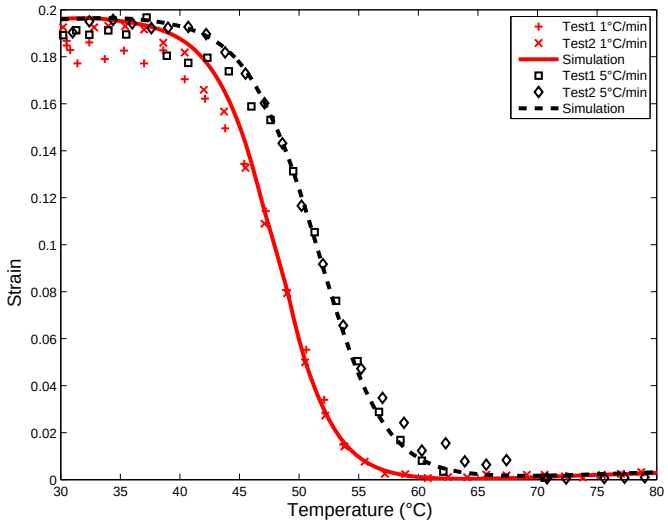

Figure 11: Comparison between model and experiments for free length recovery of 20% pre-strained samples at 65°C for 1°C/min and 5°C/min heating rates.

the experimental tests must be stored properly in order to run accurate simulations.

4.3. Discussion

The previous section has shown that our model leads to a quantitative (for free length recovery) or at least qualitative (for constrained length recovery) agreement with a large set of experimental results in various conditions. Few models have been compared to various conditions. This is the case for Castro et al. (2010), for instance, but constrained length recovery only was considered, and the lower part of the curves is missing. Both a single free length recovery and a single constrained length recovery were considered by Srivastava et al. (2010), with a weaker model-experiment agreement compared to ours. In similar conditions, Nguyen et al. (2008) obtained a poor agreement for free length recovery and the lower part of the constrained length recovery curve is missing. Free length recoveries only are considered by Yu et al. (2012), with a good agreement but for very limited cases.

All the parameters used in our model are obtained from DMA tests, tensile tests in the rubbery state and thermal expansion tests. No additional fitting is required on a shape memory experiment. The model applies to general three-dimensional loadings and is implemented in a finite element

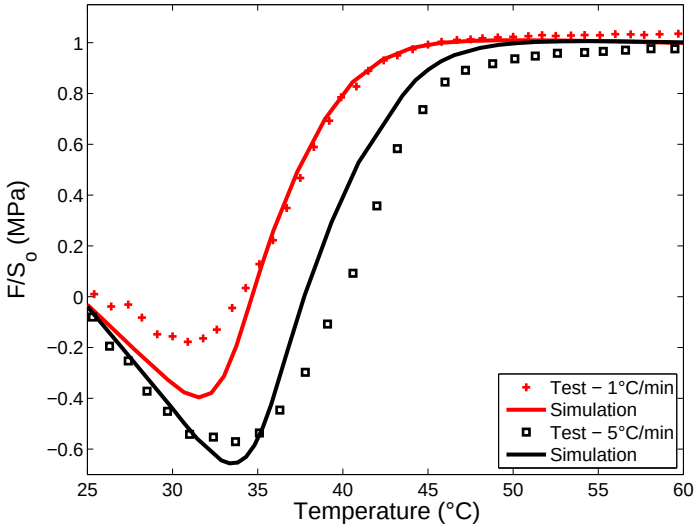

Figure 12: Comparison between model and experiments for constrained length recovery of 20% pre-strained samples at 65°C for 1°C/min and 5°C/min heating rates.

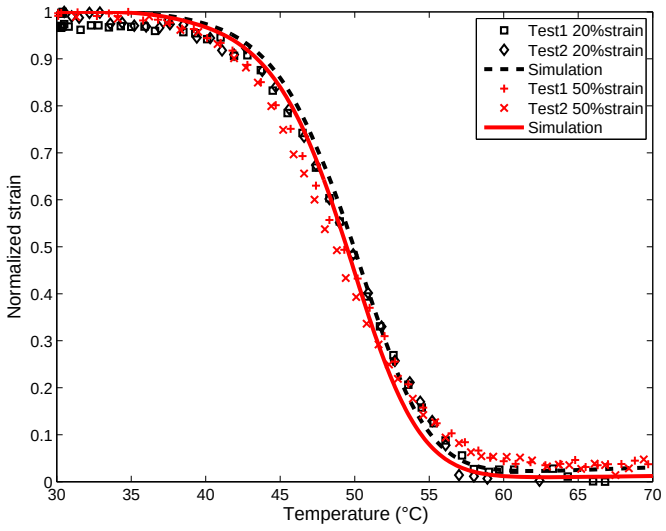

Figure 13: Comparison between model and experiments for normalized free length recovery at 45°C for 20% or 50% pre-strain and heating at 5°C/min.

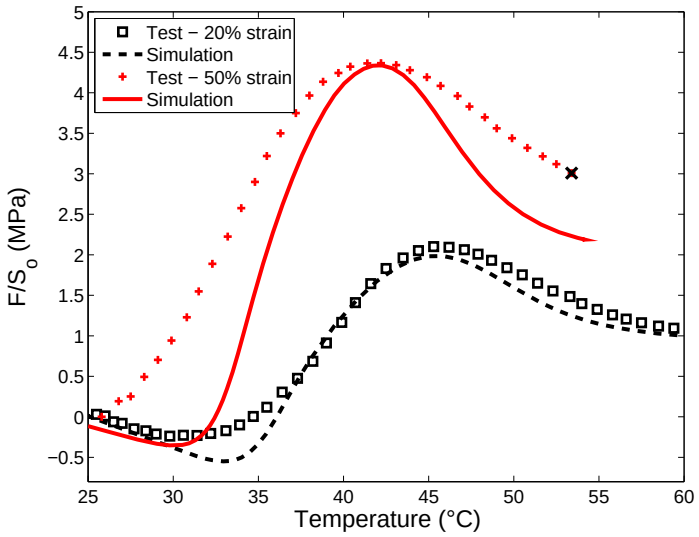

Figure 14: Comparison between model and experiments for constrained length recovery for 20% or 50% pre-strain at 45°C and heating at 1°C/min

code. These features are shared by the models of Nguyen et al. (2008) and of Srivastava et al. (2010), but the models of Castro et al. (2010) and of Yu et al. (2012) that are fitted on recovery experiments, are limited to uniaxial loadings, and cannot be used for computer-assisted design. Our model uses standard features of a commercial finite element code, whereas Srivastava et al. (2010) wrote a complex user-material subroutine and Nguyen et al. (2008) used a specific finite element code. Finally our model uses 20 Maxwell branches, identified by DMA tests, while Nguyen et al. (2008) and Castro et al. (2010) use only one, and Srivastava et al. (2010) use two (with a very large number of parameters, though). A small number of branches cannot render the complexity of a polymer behavior and may explain poor predictions of free length recovery. Yu et al. (2012) included seven Maxwell branches, but with an unrealistic equal Young modulus for all, which was not obtained from DMA tests.

In order to illustrate the model ability to predict a large range of shape memory recoveries, we have performed triple shape memory tests based on the experiments reported by Xie (2010) and modeled by Yu et al. (2012). The material was heated to 55°C (in the viscoelastic transition) and deformed 11% at this temperature (temporary shape 1), then the sample was cooled down to 40°C at constant strain. After a temperature stabilization of 5 minutes,

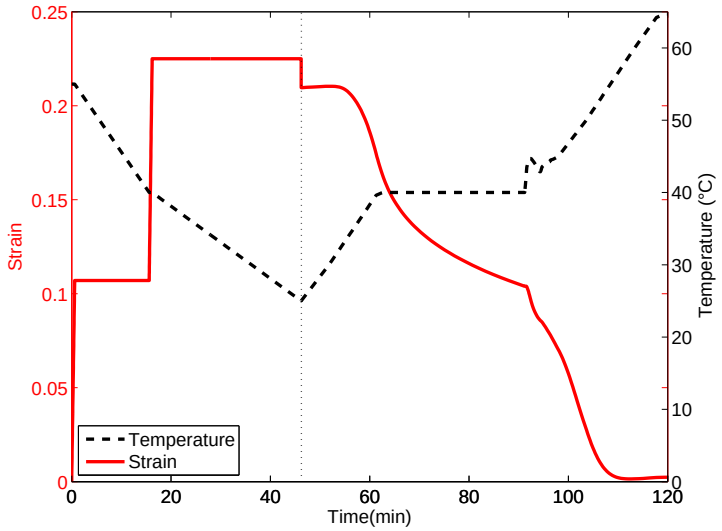

Figure 15: Triple-shape memory thermocycle for a sample deformed 11% at 55°C and 12% at 40°C

the sample was deformed by an additional 12% at 40°C (temporary shape 2), and the material was cooled down to room temperature (25°C) finally. The recovery free length phase, where the strain evolution was measured, applied a non-monotonic heating ramp: first, the temperature was raised from room temperature to 40°C at 5°C/min (first recovery), and then held constant for 30 minutes. A further heating from 40°C to 65°C at 5°C/min followed (second recovery). Figure 15 shows the prescribed temperature history and the prescribed or measured strain history. Note that the same temperature history was prescribed in the numerical simulations to obtain accurate results. Figure 16 compares the experimental and predicted strain histories during the recovery and an excellent agreement can be observed. Yu et al. (2012) used a different material and different loading conditions but with less complete model-experiment agreement for their triple-shape memory test than in Figure 16.

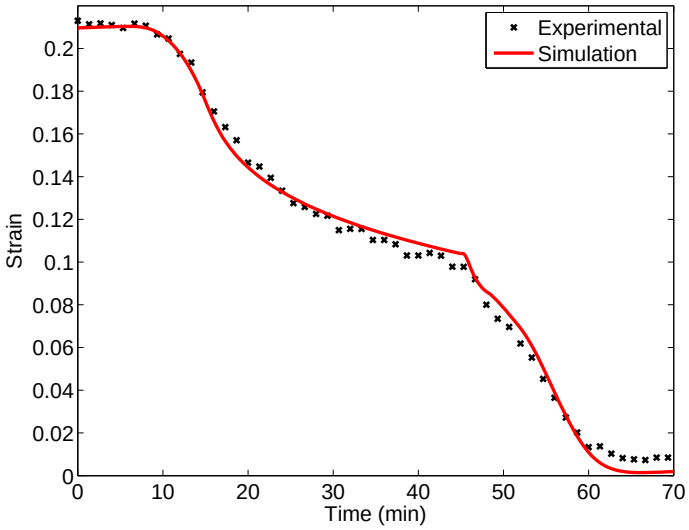

Figure 16: Triple-shape memory recovery for a sample deformed 11% at 55°C and 12% at 40°C

5. Conclusions

Shape memory recovery thermomechanical behavior prediction is fundamental for the development of shape memory polymers applications. A viscoelastic model, already validated for shape recovery of small-strain large-deformation torsion tests, has been extended to large-strain uniaxial tension. Moreover, the model was proved to predict well both free length strain recovery and constrained length stress recovery in various loading conditions. Along with providing a good prediction of the viscoelastic thermomechanical response during recovery tests, the model strength stands in its parameter characterization that requires conventional mechanical tests only, including DMA tests, linear thermal expansion tests and uniaxial tension tests in the rubbery state. The model performed extremely well when compared to the experimental data, without featuring any adjustable parameter. Moreover, the model capability to predict triple-shape recovery in addition to the classic shape memory tests has been shown. This study confirms that not only the shape recoveries but also the stress recoveries measured during classic thermomechanical tests for shape memory polymers result from the polymer viscoelasticity combined with its property of time-temperature superposition. Finally, standard features of the Abaqus finite element code can be

used easily to implement the model without additional programming, which provides a convenient tool for computer assisted design of shape memory polymer applications.

Acknowledgement

This work was supported by the French Agence Nationale de la Recherche through project REFORM 10-JCJC-0917.

Abaqus/Standard, 2010. Dassault Systems Simulia Corporation. Providence, RI, USA.

Azra, C., Plummer, C., Manson, J., 2011. Isothermal recovery rates in shape memory polyurethanes. Smart Materials and Structures 20, 082002–082011.

Castro, F., Westbrook, K., Long, K., Shandas, R., Qi, H., 2010. Effects of thermal rates on the thermomechanical behaviors of amorphous shape memory polymers. Mechanics of Time-Dependent Materials 14, 219–241.

Chen, Y., Lagoudas, C., 2008. A constitutive theory for shape memory polymers: Part II: A linearized model for small deformation. Journal of the Mechanics and Physics of Solids 56, 1766–1778.

Diani, J., Gilormini, P., Frédy, C., Rousseau, I., 2012. Predicting thermal shape memory of crosslinked polymer networks from linear viscoelasticity. International Journal of Solids and Structures 49, 793–799.

Diani, J., Liu, Y., Gall, K., 2006. Finite strain 3D thermoviscoelastic constitutive model for shape memory polymers. Polymer Engineering and Science 46, 486–492.

Feldkamp, D., Rousseau, I., 2011. Effect of the deformation temperature on the shape-memory behavior of epoxy networks. Macromolecular Materials and Engineering 295, 726–734.

Gall, K., Yakacki, C., Liu, Y., Shandas, R., Willett, N., Anseth, K., 2005. Thermomechanics of the shape memory effect in polymers for biomedical applications. Journal of Biomedical Materials Research 73A, 339–348.

Gilormini, P., Diani, J., 2012. On modeling shape memory polymers as thermoelastic two-phase composite materials. Comptes Rendus Mécanique 340, 338–348.

Leonardi, A., Fasce, L., Zucchi, I., Hoppe, C., Soul, E., Prez, C., Williams, R., 2011. Shape memory epoxies based on networks with chemical and physical crosslinks. European Polymer Journal 47, 362–369.

Liu, Y., Gall, K., Dunn, M., Greenberg, A., Diani, J., 2006. Thermomechanics of shape memory polymers: Uniaxial experiments and constitutive model. International Journal of Plasticity 22, 279–313.

Nguyen, T., Qi, H., Castro, F., Long, K., 2008. A thermoviscoelastic model for amorphous shape memory polymers: Incorporating structural and stress relaxation. Journal of the Mechanics and Physics of Solids 56, 2792–2814.

Qi, H., Nguyen, T., Castro, F., Yakacki, C., Shandas, R., 2008. Finite deformation thermo-mechanical behavior of thermally-induced shape memory polymers. Journal of the Mechanics and Physics of Solids 56, 1730–1751.

Rousseau, I., Xie, T., 2010. Shape memory epoxy: Composition, structure, properties and shape memory performances. Journal of Materials Chemistry 20, 3431–3441.

Safransky, D., Gall, K., 2008. Effect of chemical structure and crosslinking density on the thermo-mechanical properties and toughness of (meth)acrylate shape memory polymer networks. Polymer 49, 4446–4455.

Simo, J., 1987. On a fully three dimensional finite strain viscoelastic damage model: Formulation and computational aspects. Computer Methods in Applied Mechanics and Engineering 60, 153–173.

Smith, T., 1963. Ultimate tensile properties of elastomers. l. characterization by a time and temperature independent failure envelope. Journal of Polymer Science Part A 1, 3597–3615.

Srivastava, V., Chester, S., Anand, L., 2010. Thermally actuated shape memory polymers: Experiments, theory, and numerical simulations. Journal of the Mechanics and Physics of Solids 58, 1100–1124.

Tobushi, H., Hashimoto, H., Hayashi, S., Yamada, E., 1997. Thermomechanical constitutive model of shape memory polymer of polyurethane series. Journal of Intelligent Material Systems and Structures 8, 711–718.

Volk, B., Lagoudas, D., Chen, Y., 2010. Analysis of the finite deformation response of shape memory polymers: 1D calibration and numerical implementation of a finite deformation, thermoelastic model. Smart Materials and Structures 19, 075006–075016.

Weese, J., 1993. A regularization method for nonlinear ill-posed problems. Computational Physics Community 77, 429–440.

Williams, M., Landel, R., Ferry, J., 1955. The temperature dependence of relaxation mechanisms in amorphous polymers and other glass-forming liquids. Journal of the American Chemical Society 77, 3701–707.

Xie, T., 2010. Tunable polymer multi-shape memory effect. Nature 464, 267–270.

Yackaki, C., Willis, S., Luders, C., Gall, K., 2008. Deformation limits in shape memory polymers. Advanced Engineering Materials 10, 112–119.

Yu, K., Xie, T., Leng, L., Ding, Y., Qi, J., 2012. Mechanisms of multi-shape memory effects and associated energy release in shape memory polymers. Soft Matter 8, 5687–5695.

Appendix: Material parameters

Implementation of the mechanical behavior in the Abaqus input file:

```
*MATERIAL,NAME=POLYM
*HYPERELASTIC,NEO HOOKE,MODULI=INSTANTANEOUS
1.0973E+08,1.7450E-09
*VISCOELASTIC,TIME=PRONY
1.8706E-01,0,1.26E-06
1.5840E-01,0,2.94E-06
1.3761E-01,0,6.87E-06
1.2378E-01,0,1.60E-05
1.1283E-01,0,3.75E-05
9.8684E-02,0,8.75E-05
```

```
7.5819E-02,0,2.04E-04
4.7521E-02,0,4.78E-04
2.4477E-02,0,1.12E-03
1.1651E-02,0,2.61E-03
5.8277E-03,0,6.08E-03
3.1949E-03,0,1.42E-02
1.8477E-03,0,3.32E-02
1.0527E-03,0,7.75E-02
5.6387E-04,0,1.81E-01
2.8586E-04,0,4.23E-01
1.4378E-04,0,9.88E-01
7.4217E-05,0,2.31E+00
3.9113E-05,0,5.39E+00
2.0746E-05,0,1.26E+01
*TRS,DEFINITION=WLF
80.,6.9,87.9
```

Followed by:

```
*EXPANSION
9.1718E-05,20
9.5553E-05,25
9.9354E-05,30
1.0520E-04,35
1.1222E-04,40
1.2083E-04,45
1.3032E-04,50
1.3899E-04,55
1.4697E-04,60
1.5258E-04,65
1.5652E-04,70
1.5943E-04,75
```

for thermal expansion at 1°C/min or

```
*EXPANSION
1.1741E-04,20
1.2162E-04,25
1.2589E-04,30
1.3229E-04,35
1.4066E-04,40
1.4997E-04,45
```

```
1.5868E-04,50
1.6658E-04,55
1.7326E-04,60
1.7811E-04,65
1.8170E-04,70
1.8425E-04,75
```

for thermal expansion at 5°C/min.